Electronic Transitions in Slow Collisions of Atoms and Molecules. III. Eikonal Approximation for Nonclassical Scatterings*

Joseph C. Y. Chen and Chen-Show Wang†
Department of Physics and Institute for Pure and Applied Physical Sciences, University of California, San Diego, La Jolla, California 92037

and

Kenneth M. Watson
Department of Physics and Lawrence Radiation Laboratory, University of California, Berkeley, California 94720
(Received 20 October 1969)

Characteristic quantum features in atomic collisions are analyzed in the eikonal approximations. Numerical illustrations are given for the (He^+, He) system, using a set of model potentials which provide a reasonable description of the interaction between the ground states of He^+ and He in the quasiadiabatic (diabatic) limit.

I. INTRODUCTION

In paper I of this series, [1] a method for studying rearrangement collisions between atoms and molecules was formulated. It was shown that the use of the eikonal approximation permits the coupled equations of collision theory to be reduced to one-dimensional equations defined along classical trajectories. In paper II of this series, [2] this approach was further developed. Several practical techniques for evaluating wave functions and Green's functions were introduced. Numerical illustrations of these techniques were carried out, particularly for the (H^+, H) collision system, in the classical limit of the eikonal approximation. In this paper, we are concerned with the application of the eikonal approximation to collisions where a classical description fails. The problem of nonadiabatic transitions will be considered in paper IV of this series.

Before beginning the application to nonclassical collisions, it is useful to review and compare the criteria for the validity of the classical and eikonal description of collisions. We will again consider cases where the potential energies of interaction have ranges of order a_0(the Bohr radius)

$$\lim_{R/a_0\to\infty} V(R) \leq O(1/R^{1+\delta}) \ , \qquad \delta > 0 \tag{1.1}$$

and have strengths of order 1 Ry, recognizing that V may be singular at $R = 0$.

The error resulting from the use of the eikonal approximation may be estimated from the correction factor [Eq. (II A. 2)] for the amplitude $A(R)$ [Eq. (II 1. 8c)] of the eikonal wave function $\psi(\vec{R})$ [Eq. (II 1. 8a)] or from the propagation amplitude $A(\vec{R}, \vec{R}')$[Eq. (II 6. 3)] of the Green's function $\langle \vec{R}|G|\vec{R}'\rangle$ [Eq. (II 1. 12)] in the eikonal approximation. This gives, except for certain singular regions in the asymptotic domain, an error of order [Eq. (II 1. 14)]

$$\eta(\text{eik}) \approx \left|\hbar\Theta_c/pa_0\right| \sim (920A_{\text{eff}}E^3)^{-1/2} \ , \tag{1.2}$$

with $$M/m = 920A_{\text{eff}} \ , \tag{1.3}$$

where Θ_c is the classical scattering angle, M is the reduced mass of the colliding particles, and m is the mass of the electron. At energies $\epsilon_p \equiv p^2/2M$, much larger than the Rydberg energy, it is clear that, for particles of atomic mass, we have

$$\eta(\text{eik}) \ll 1 \ . \tag{1.4}$$

The error resulting from the classical description of the collisions, on the other hand, is of order [Eqs. (II 5. 19) and (II 1. 25)]

$$\eta(\text{class}) = \frac{d^2\Theta_c}{db^2}\left(p^{1/2}\left|\frac{d\Theta_c}{db}\right|^{3/2}\right)^{-1} \sim \left(\frac{E}{920A_{\text{eff}}}\right)^{1/2}, \tag{1.5}$$

where b is the impact parameter. The criterion,

$$\eta(\text{class}) \ll 1 \ ,$$

gives, therefore, an upper bound to the c.m. energy for the validity of the classical description.

II. EIKONAL APPROXIMATION FOR SCATTERING AMPLITUDE

The analysis of collisions is appreciably simpli-

fied when the conditions are satisfied for the eikonal approximation[1] [Eq. (1.4)]. In this case, the collision may be described by the eikonal wave function [Eqs. (I 4.8) and (I 4.35)]

$$\Psi(\vec{R}) = (2\pi)^{-3/2} A(\vec{R})\, e^{iS(\vec{R})}, \tag{2.1}$$

where $S(\vec{R})$ is the eikonal

$$S(\vec{R}) = \int^{\vec{R}} \kappa(\vec{R}')\, ds \tag{2.2}$$

$$\kappa^2 = p^2 - 2MV(R)\,, \tag{2.3}$$

$$\text{and } A(\vec{R}) = \left(\frac{p}{\kappa}\right)^{1/2} \left\{ \exp\left[-\frac{1}{2} \int^{\vec{R}} \left(\frac{1}{\mathcal{R}_1} + \frac{1}{\mathcal{R}_2} \right) ds \right] \right\}. \tag{2.4}$$

Here ds is an element of path length, p is the magnitude of the relative momentum of the colliding particles, $\mathcal{R}_1$ and $\mathcal{R}_2$ are the principal radii of curvature of the surface of constant eikonal which passes through $\vec{R}$, and the path integrals are taken along the classical trajectory.

When the eikonal wave function is utilized, the T matrix for scattering from an asymptotic momentum $\vec{p}$ into an asymptotic momentum $\vec{k}$ may be written to order η(eik) as[2]

$$T = (2\pi)^{-3} \int d^3R\, V(R) A(\vec{R}) \times \exp\{ i[S_{\vec{p}}^{+}(\vec{R}) - \vec{k}\cdot\vec{R}\,] \}\,. \tag{2.5}$$

This integral expression for T can be evaluated in approximations which are consistent with the eikonal approximation.

Following paper II, we write, for the eikonal, the expression [Eq. (II 1.19)]

$$S(\vec{R}) = S_0 + S_1 + S_2 + O(\eta_S), \tag{2.6}$$

$$\text{where } \eta_S \equiv p a_0 |\theta_c|^3 \approx [920 A_{\text{eff}}/E^5]^{1/2}. \tag{2.7}$$

[The approximation in which S_2 is neglected in Eq. (2.6) for $S(\vec{R})$, is called the straight-line approximation.[3]] If we suppose that in addition to η_S, the quantity

$$\eta_O \equiv p a_0 \theta^3 \tag{2.8}$$

is also small, $(S_{\vec{p}}^{+}(\vec{R}) - \vec{k}\cdot\vec{R})$ in Eq. (2.5) takes the form [Eq. (II 5.6)], in the classical limit,

$$S_{\vec{p}}^{+}(\vec{R}) - \vec{k}\cdot\vec{R} = \Phi(\bar{z}, b) - pb\sin\theta\cos\varphi\,, \tag{2.9}$$

$$\text{with } \Phi(\bar{z}, b) = -p \int_{-\infty}^{\bar{z}} \{ \tfrac{1}{2}[\beta^2 - \beta^2(\bar{z}')] + U(\bar{R}) \} d\bar{z}'\,, \tag{2.10}$$

$$U(R) \equiv 1 - [1 - V(R)/\epsilon_p]^{1/2}, \tag{2.11}$$

where $\beta(\bar{z})$ is the angle between the tangent vector $\hat{\kappa}(\bar{z})$ and the $\bar{z}$ axis, $\beta = \lim \beta(\bar{z})$, as $\bar{z} \to \infty$ is the asymptotic angle, and φ is the azimuthal angle in a cylindrical coordinate system with a volume element

$$d^3R = \rho d\rho\, dz\, d\varphi\,. \tag{2.12}$$

The T matrix then takes the approximate form

$$T = (2\pi)^{-3} \int \rho d\rho\, dz\, d\varphi\, V(R) A(\vec{R}) \times e^{-ipb\sin\theta\cos\varphi}\, e^{i\Phi(\bar{z}, b)}\,. \tag{2.13}$$

It should be noted that this expression for T remains valid when the classical limit is not valid. This is because the following inequalities:

$$\theta_c^2 p a_0 \ll 1, \quad \theta^2 p a_0 \ll 1, \quad \text{and} \quad \theta\,|\theta_c| p a_0 \ll 1$$

are satisfied when the classical limit fails as $|\theta_c| p a_0$ becomes comparable to unity.

To relative order $|\theta_c|$ we may set, for the amplitude $A(\vec{R})$ for the eikonal wave function,

$$A(\vec{R}) = 1\,, \tag{2.14}$$

and take the following approximations:

$$\rho\, d\rho\, dz \cong b\, db\, d\bar{z}\,, \tag{2.15}$$

$$V(R) d\bar{z} \cong -(p/M) d\Phi\,. \tag{2.16}$$

This then permits us to write

$$T = -[v/(2\pi)^3] \int b\, db\, d\Phi\, e^{i\Phi} \int d\varphi\, e^{-ipb\sin\theta\cos\varphi}\,,$$

where $v \equiv p/M$ is the asymptotic relative velocity. We then obtain the expression [Eq. (II 5.11)]

$$T = -[v/i(2\pi)^2] \int_0^{\infty} b\, db\, J_0(pb\sin\theta)(e^{i\Phi(b)} - 1)\,, \tag{2.17}$$

$$\text{where } \Phi(b) \equiv \lim \Phi(\bar{z}, b)\,, \quad \text{as } \bar{z} \to \infty\,. \tag{2.18}$$

This is the expression we will use for the analysis of the characteristic quantum features in atomic collisions.

III. APPLICATION TO NONCLASSICAL COLLISIONS

In this section, the approximate method described in Secs. I and II is applied to a system with the following set of interaction potentials (in rydberg units):

$$V_u(R)=\frac{\alpha_1}{R}e^{-\delta_1 R}-\alpha_2 R^2 e^{-\delta_2 R} \quad , \tag{3.1}$$

$$V_g(R)=V_u(R)+\alpha_3 e^{-\delta_3 R} \quad , \tag{3.2}$$

where $\alpha_1=7.9989$, $\alpha_2=1.219$, $\alpha_3=9.55531$, $\delta_1=2.1696$, $\delta_2=1.56105$, and $\delta_3=1.253921$. This set of potentials provides a reasonable description for the interaction between the ground states of He^+ and He in the quasiadiabatic (diabatic) limit. A detailed investigation of these potentials is given in Appendix A where comparisons of the theoretical results (based on these potentials) with experimental He^+-on-He measurements are made for differential scattering and electron-transfer cross sections. In this section, we will treat the system with the above set of potentials as a model (He^+, He) system.

The differential scattering and electron-transfer cross sections are given, respectively, by

$$\frac{d\sigma_s}{d\Omega}=\frac{d\sigma_g}{d\Omega}+\frac{d\sigma_u}{d\Omega}+\frac{d\sigma_I}{d\Omega} \quad , \tag{3.3}$$

$$\frac{d\sigma_{et}}{d\Omega}=\frac{d\sigma_g}{d\Omega}+\frac{d\sigma_u}{d\Omega}-\frac{d\sigma_I}{d\Omega} \quad , \tag{3.4}$$

with

$$\frac{d\sigma_g}{d\Omega}=4\pi^4 M|T_g|^2 \quad , \tag{3.5}$$

$$\frac{d\sigma_u}{d\Omega}=4\pi^4 M|T_u|^2 \quad , \tag{3.6}$$

$$\frac{d\sigma_I}{d\Omega}=8\pi^4 M\mathrm{Re}(T_g^* T_u) \quad , \tag{3.7}$$

where $d\sigma_g/d\Omega$, $d\sigma_u/d\Omega$, and $d\sigma_I/d\Omega$ correspond to the contributions to the cross sections from the *gerade* interaction (V_g), the *ungerade* interaction (V_u) and their interference, respectively. In the eikonal approximation the T matrix is given by Eq. (2.17) to the order of $O(\eta_S)$ [see Eq. (2.7)]. This integral expression for the T matrix is evaluated for the model potentials for several limiting cases.

When the condition for the classical description is satisfied, the integral may be evaluated by the stationary-phase approximation

$$\theta=|\Theta_c(b_c)| \quad , \tag{3.8}$$

where b_c is the impact parameter at the point of the stationary phase and Θ_c is the classical scattering angle. This then leads to the classical scattering matrix [Eq. (II 5.20)]

$$T\cong-(4\pi^2 M)^{-1}\left(\frac{b_c}{\sin\theta}\left|\frac{db_c}{d\theta}\right|\right)^{1/2} \times\exp\{i[\Phi(b_c)-e_1(b_c)pb_c\theta]\} \times\exp\left[i\frac{\pi}{4}\left(e_1(b_c)-2+\frac{d\Theta_c}{db_c}\Big/\left|\frac{d\Theta_c}{db_c}\right|\right)\right] \quad , \tag{3.9}$$

where we have defined $e_1(b)\equiv\Theta_c(b)/|\Theta_c(b)|$.

The *ungerade* potential $V_u(R)$ given by Eq. (3.1) is not a simple monotomic attractive potential and is capable of giving rise to several points of stationary phase. This then gives rise to interesting interference patterns. As long as these points of stationary phase are well separated, the scattering observed at an angle θ may be calculated from the sum of the contributions coming from impact parameters at these points of stationary phase:

$$T_u=\sum_j T_{ju} \quad , \tag{3.10}$$

where the sum over j sums over all the participating impact parameters.

The model potentials given by Eqs. (3.1) and (3.2) have the advantage of permitting the integrals which appear in $\Phi(b)$, $\Theta_c(b)$, $d\Theta_c/db$, etc., to be evaluated analytically in the straight-line and angle approximations for the trajectory. For example, the classical scattering angle for the *ungerade* mode of interaction takes, to the order of $O(\theta_c^2)$, the form

$$\Theta_c^{(u)}(b)\cong\theta_c^{(u)}(b)=\xi^2(m/M) \times[\alpha_1\delta_1 K_1(\delta_1 b_u)+\alpha_2 b_u^2 K_1(\delta_2 b_u)-\alpha_2\delta_2 b_u^3 K_0(\delta_2 b_u)] \tag{3.11}$$

with $$\xi=(\hbar/a_0 p)(M/m) \quad ,$$

where ξ is a dimensionless quantity and $K_\nu(z)$ is the modified Bessel function of order ν and argument z.

$$K_\nu(z)=\frac{\pi^{1/2}}{\Gamma(\nu+\frac{1}{2})}\left(\frac{z}{2}\right)^\nu\int_0^\infty e^{-z\cosh t}(\sinh t)^{2\nu}dt \quad . \tag{3.12}$$

The results of the calculation is shown in Figs. 1–3 for three different c.m. energies. To assess

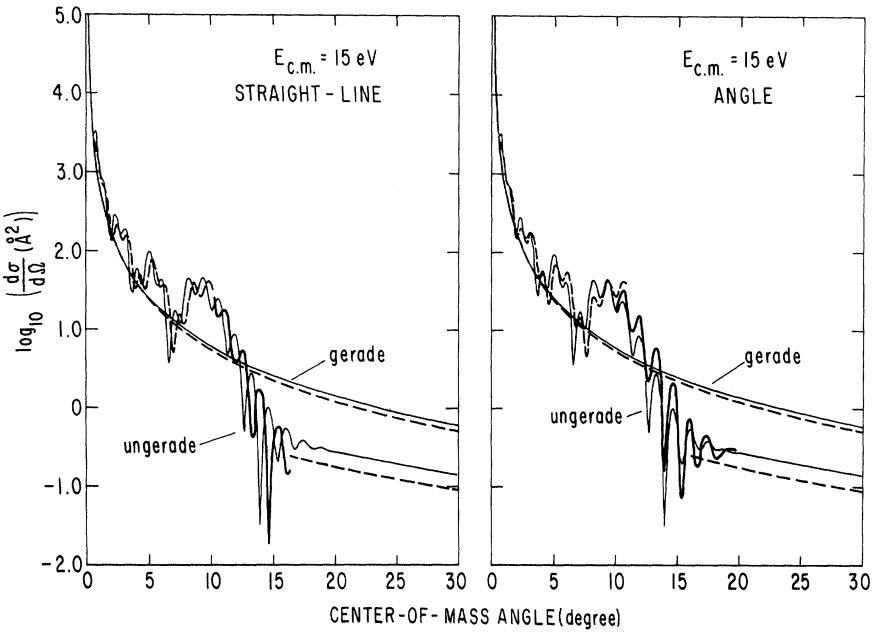

FIG. 1. Comparison of the differential cross sections for the gerade- and ungerade-potential scatterings in the absence of the nuclear symmetry as functions of c.m. angle in the WKB (solid line); the stationary-phase (dashed line) and the eikonel (bold-face solid line) approximations for a model (He^+, He) system [Eqs. (3.1) and (3.2)] at an energy of 15 eV in the c.m. system. Calculations for the latter two approximations are reported for both the straight-line and angle approximations for the classical trajectories.

the reliability of the classical approximation, we have included in these figures the results of the WKB approximation using these potentials by summing over all the significant partial-wave contributions. It is seen that the classical approximation gives a very reasonable description of the multipath interference on the bright side ($\theta < \theta_r$) of the rainbow angle θ_r. On the dark side of the rainbow angle ($\theta > \theta_r$), the agreement between the WKB and the classical approximation is no longer as encouraging as for the bright side. The angle approximation for the trajectory, nevertheless, yields results which are in better agreement with the WKB results. The inclusion of nuclear symmetry does not change this observation as shown in Figs. 4–6. The classical approximation, however, over exaggerates the nuclear-symmetry oscillations.

The "angle" approximation which is described in

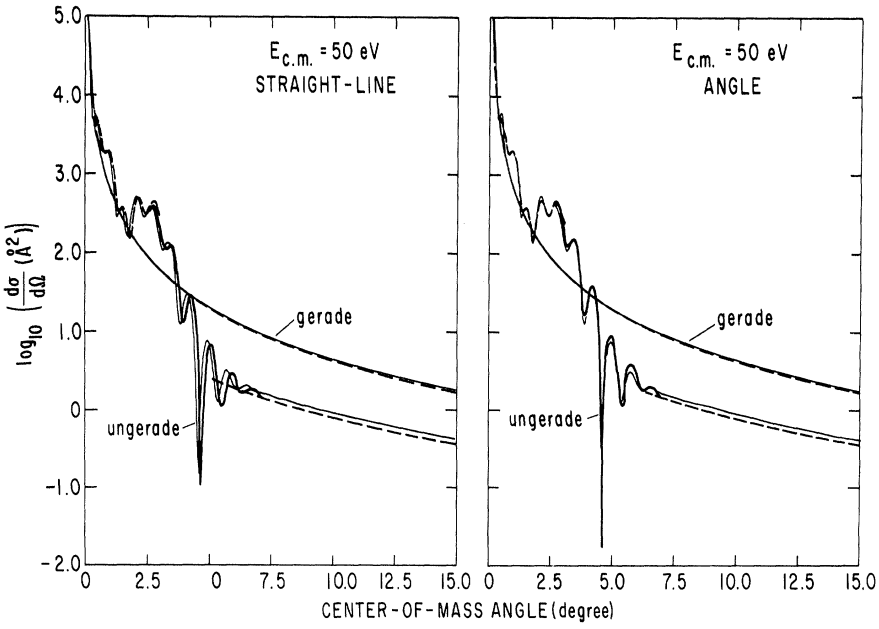

FIG. 2. Comparison of the differential cross sections for the gerade- and ungerade-potential scatterings in the absence of the nuclear symmetry as functions of c.m. angle in the WKB (solid line); the stationary-phase (dashed line) and the eikonel (bold-face solid line) approximations for a model (He^+, He) system [Eqs. (3.1) and (3.2)] at an energy of 50 eV in the c.m. system. Calculations for the latter two approximations are reported for both the straight-line and angle approximations for the classical trajectories.

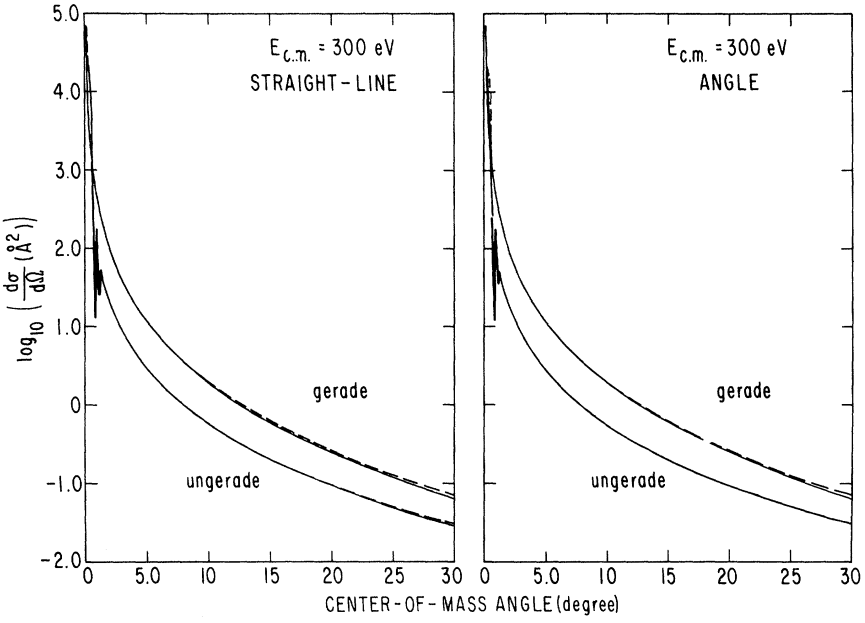

FIG. 3. Comparison of the differential cross sections for the gerade- and ungerade-potential scatterings in the absence of the nuclear symmetry as functions of c.m. angle in the WKB (solid line), the stationary-phase (dashed-line) and the eikonel (bold face solid line) approximations for a model (He^+, He) system [Eqs. (3.1) amd (3.2)] at an energy of 300 eV in the c.m. system. Calculations for the latter two approximations are reported for both the straightline and angle approximations for the classical trajectories.

paper II differs from the straight-line approximation only by the addition of the term $\delta\Phi$ in the phase Φ.

$$\delta\Phi = \xi b V(d) \tan(\tfrac{1}{2}\theta_c) \ , \qquad (3.13)$$

with

$$d \cong b/\cos(\tfrac{1}{2}\theta_c) \ , \qquad (3.14)$$

where V is in rydbergs and b is in Bohr radii. It is interesting that this simple modification provides a significant improvement over the straight-line approximation even at moderately large scattering angles.

The classical scattering matrix provides no information for rainbow scatterings and for the forward and backward (glory) scatterings. This is due to the vanishing of $d\theta/dL$ and $\sin\theta$, respectively. For these cases, the integral expression for the T matrix must be evaluated. Before carrying out the numerical evaluation, it is instructive to examine some approximate expressions[4,5] which may be derived from Eq. (2.17) near the

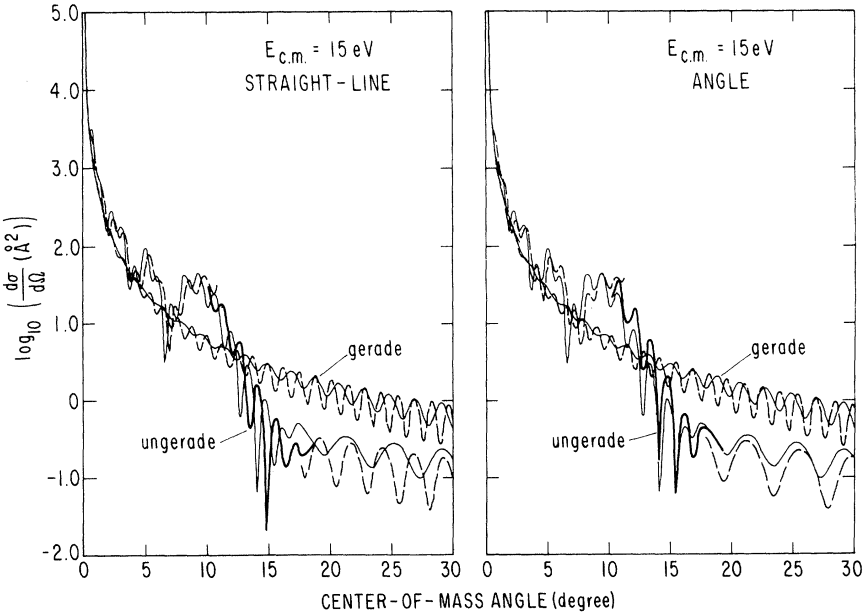

FIG. 4. Comparison of the differential cross sections for the gerade- and ungerade-potential scatterings as functions of c.m. angle in the WKB (solid line), the stationary-phase (dashed line) and the eikonel (bold-face solid line) approximations for a model (He^+, He) system [Eqs. (3.1) and (3.2)] at an energy of 15 eV in the c.m. system. Calculations for the latter two approximations are reported for both the straight-line and angle approximations for the classical trajectories.

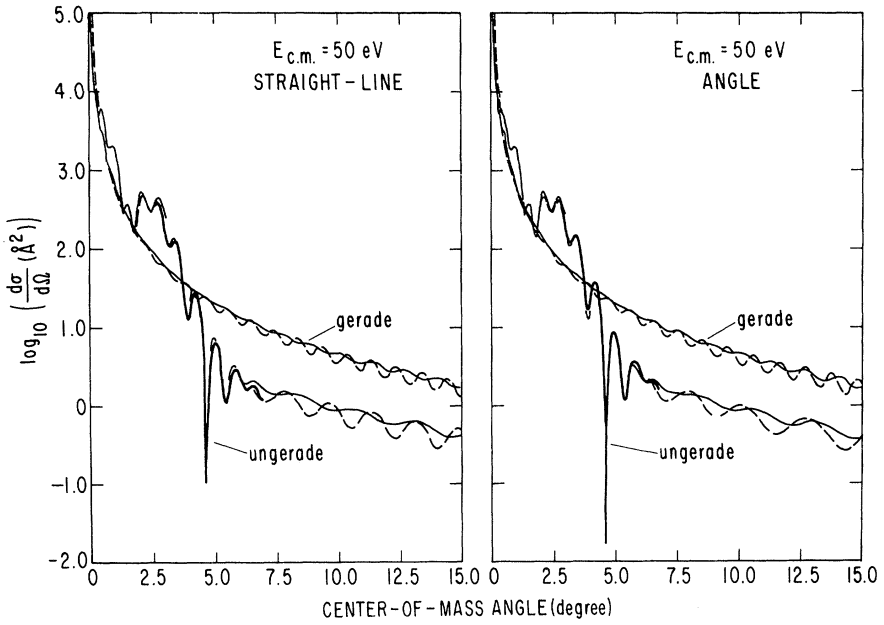

FIG. 5. Comparison of the differential cross sections for the gerade- and ungerade-potential scatterings as functions of c.m. angle in the WKB (solid line), the stationary-phase (dashed line) and the eikonel (bold-face solid line) approximations for a model (He^+, He) system [Eqs. (3.1) and (3.2)] at an energy of 50 eV in the c.m. system. Calculations for the latter two approximations are reported for both the straight-line and angle approximations for the classical trajectories.

rainbow and the forward and backward scatterings.

Near a rainbow angle θ_r, the phase $\Phi(b)$ may be expanded in terms of the Taylor's series near the rainbow impact parameter b_r which is defined by the relation

$$\theta_r = |\Theta_c(b_r)| \ . \tag{3.15}$$

We have

$$\Phi(b) \cong \Phi(b_r) + p\Theta_c(b_r)(b - b_r) + \tfrac{1}{6}p(d^2\theta_c/db_r)(b - b_r)^3. \tag{3.16}$$

Substitution of Eq. (3.16) into Eq. (2.17) yields

$$T \cong -\frac{v}{4\pi^2}\frac{\exp\{i[\gamma(b_r) - e_1(b_r)\frac{1}{4}\pi]\}}{[2\pi p \sin\theta]^{1/2}} \times \int_0^\infty b^{1/2}db \exp\{ip\left[[\Theta_c(b_r) - e_1(b_r)\theta] \times (b - b_r) + \frac{1}{6}\left(\frac{d^2\Theta_c}{db_r^2}\right)(b - b_r)^3\right]\}, \tag{3.17}$$

with $$\gamma(b_r) = \Phi(b_r) - e_1(b_r)pb_r\theta \ , \tag{3.18}$$

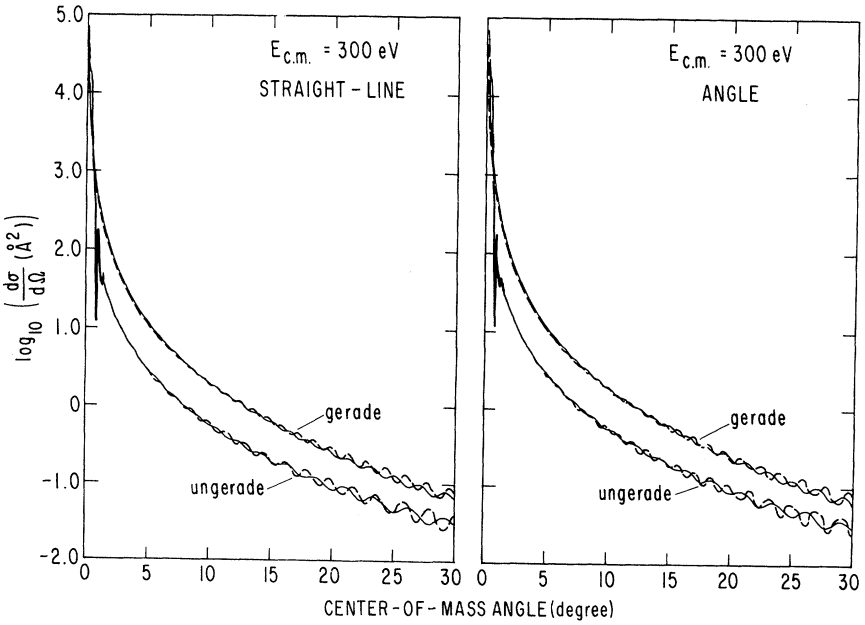

FIG. 6. Comparison of the differential cross sections for the gerade- and ungerade-potential scatterings as functions of c.m. angle in the WKB (solid line), the stationary-phase (dashed line) and the eikonel (bold-face solid line) approximations for a model (He^+, He) system [Eqs. (3.1) and (3.2)] at an energy of 300 eV in the c.m. system. Calculations for the latter two approximations are reported for both the straight-line and angle approximations for the classical trajectories.

where we have utilized the asymptotic form for the Bessel function.

The integral in Eq. (3.17) may be expressed in terms of the Airy integrals[6]

$$\mathrm{Ai}(z)=\frac{1}{2\pi}\int_{-\infty}^{\infty}\exp(izt+\tfrac{1}{3}it^3)dt \quad ; \tag{3.19}$$

we have from Eq. (3.17)

$$T\cong\frac{1}{4\pi^2M}\left(\frac{pb_r}{2\pi\sin\theta}\right)^{1/2}\frac{2}{p}\left(\frac{d^2\Theta_c}{db_r^2}\right)^{-1/3}$$

$$\times\mathrm{Ai}(z_r)\exp\{i[\gamma(b_r)-e_1(b_r)\tfrac{1}{4}\pi]\} \quad , \tag{3.20}$$

where

$$z_r=p\left(\frac{2}{p}\frac{d^2\Theta_c}{db_r^2}\right)^{-1/3}[\Theta_c(b_r)-e_1(\theta)] \quad . \tag{3.21}$$

The expression for T given by Eq. (3.20) has been investigated by Airy[6] for the corresponding problems in optics. It is found that the Airy integral, on the bright side of the rainbow angle, has an oscillatory behavior and, on the dark side, it falls off rapidly. This is the characteristic feature of rainbow scattering.

For forward and backward scatterings, the integral for the T matrix may also be evaluated for those values of the impact parameter which contribute most to the glory. We consider, for definiteness, a backward glory. The phase $\Phi(b)$ near π may be approximated by the expression

$$\Phi(b)\cong\Phi(b_\pi)+p\pi(b-b_\pi)+\tfrac{1}{2}p(d\Theta_c/db_\pi)(b-b_\pi)^2 \quad . \tag{3.22}$$

Substitution of Eq. (3.22) into Eq. (2.17) yields

$$T\cong i\frac{v}{4\pi^2}\exp\{i[\Phi(b_\pi)-\pi pb_\pi]\}\int_0^\infty b\,db$$

$$\times\exp\{i[\pi pb+\tfrac{1}{2}p\left(\frac{d\theta}{db_\pi}\right)(b-b_\pi)^2]\}J_0(pb\sin\theta) \quad . \tag{3.23}$$

Utilizing an integral representation for $J_0(pb\theta)$, Eq. (3.23) takes the approximate form[4]

$$T\cong\frac{1}{4\pi^2M}\left(\frac{2\pi pb^2}{d\theta/db_\pi}\right)^{1/2}J_0(pb_\pi\sin\theta)$$

$$\times\exp\left\{i\left[\Phi(b_\pi)-\pi pb_\pi-\tfrac{1}{4}\pi\left(\frac{d\Theta_c}{db_\pi}\Big/\left|\frac{d\Theta_c}{db_\pi}\right|\right)\right]\right\} \quad . \tag{3.24}$$

For the forward glory, a similar expression without the πpb_π term (in the total phase) may be obtained. From these expressions one expects, because of $J_0(pb\sin\theta)$, oscillations in the glory.

Having examined the qualitative features of a rainbow and the forward and backward glories, we now proceed with a more accurate numerical evaluation of the integral for the T matrix, Eq. (2.17). We divide the integral, for numerical accuracy, into many small segments

$$\int_0^\infty J_0(pb\sin\theta)(e^{i\Phi(b)}-1)b\,db$$

$$=\sum_j\int_{b_j}^{b_{j+1}}J_0(pb\sin\theta)(e^{i\Phi(b)}-1)b\,db$$

$$=\sum_j\left(\frac{b_j}{p\theta}J_1(pb_j\sin\theta)-\frac{b_{j+1}}{p\theta}J_1(pb_{j+1}\sin\theta)\right.$$

$$\left.+\int_{b_j}^{b_{j+1}}J_0(pb\sin\theta)e^{i\Phi(b)}b\,db\right) \quad . \tag{3.25}$$

The last integral in Eq. (3.25 is evaluated numerically with $\Phi(b)$ approximated by the expansion

$$\Phi(b)\cong\Phi(b_{j+1/2})+p\Theta_c(b_{j+1/2})(b-b_{j+1/2})$$

$$+\tfrac{1}{2}p\frac{d\Theta_c}{db_{j+1/2}}(b-b_{j+1/2})^2+\cdots \quad , \tag{3.26}$$

where $b_{j+1/2}=\frac{1}{2}(b_j+b_{j+1})$.

Calculations have been carried out for both the straight-line and "angle" approximations for the trajectory. The results for the *gerade* and *ungerade* contributions to the differential cross sections are shown in Figs. 1–6 for the rainbow and forward glory. It is seen that the integral results agree reasonably well with the WKB results. The angle approximation again predicts results which are in closer agreement with the WKB results. At regions outside of the rainbow and glory, the integral results become close to the results predicted by the classical approximation.

We have also compared the numerical results of the integral with its limiting approximations given by Eqs. (3.20) and (3.24) and found that these approximations are reasonable only in the immediate neighborhood of a rainbow and glory, respectively.

Comparisons of the various approximations for the differential scattering and electron-transfer cross sections are displayed in Figs. 7–9. It is seen that the classical approximation is reasonable for small angles on the bright side of the rainbow.

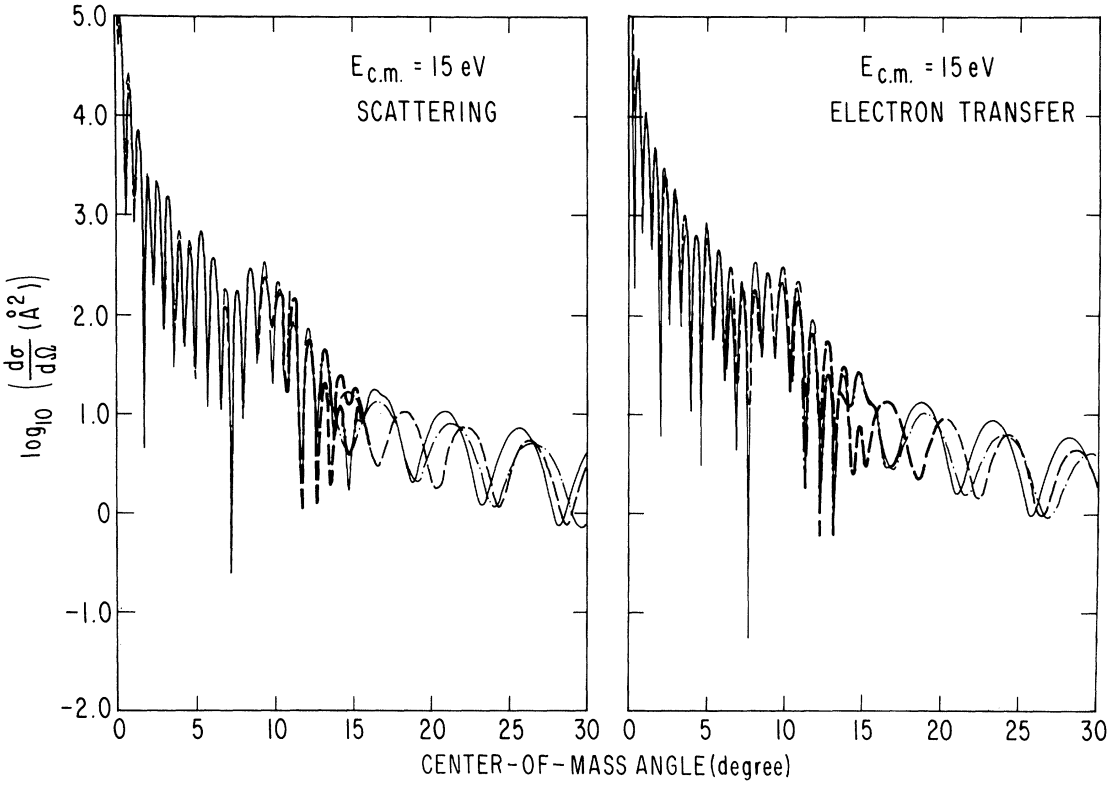

FIG. 7. Comparison of the scattering and electron-transfer differential cross sections in the absence of nuclear symmetry as functions of c.m. angle in the WKB approximation (solid line), the stationary-phase approximation with straight-line (dashed line) and angle (dot-dash line) approximations for the classical trajectory, and the eikonel approximation with straight-line (bold-face dashed line) and angle (bold-face dot-dash line) approximations for the classical trajectory for a model (He^+, He) system [Eqs. (3.1) and (3.2)] at c.m. energy of 15 eV. The differential cross sections are given in the laboratory system.

On the dark side of the rainbow the classical approximation becomes less reliable in particular if the straight-line approximation is adopted for the trajectory. The angle approximation, on the other hand, appears reasonable on the dark side of the rainbow scattering. The agreement, however, decreases with increasing angle. In the rainbow scattering region, the angle approximation is again more accurate than the straight-line approximation. The quantitative features of these various approximations remain the same when the nuclear symmetry is included in the calculation. This is shown in Figs. 10 and 11.

A comparison of the electron-transfer probability for the various approximations is given in Fig. 12. The agreement of the WKB results with the integral and classical result is again reasonably good with the angle approximation for the trajectory.

Through this study, it becomes clear that the analysis of scattering can be appreciably simplified when the conditions are satisfied for a classical and eikonal description.

APPENDIX A: INTERACTION POTENTIAL BETWEEN THE GROUND STATES OF He^+ AND He

For the interaction between the ground states of He^+ and He we have, in the adiabatic approximation, a *gerade* and an *ungerade* potential energy of interaction corresponding to the He_2^+ lowest $^2\Sigma_u^+$ and $^2\Sigma_g^+$ adiabatic electronic states. Several calculations tions for these states have been made.[7] The He_2^+ lowest $^2\Sigma_u^+$ state is in the $(1\sigma_g)^2(1\sigma_u)$ molecular configuration and approaches in the united-atom limit the $Be^+(1s)^2(2p)$ atomic state. The He_2^+ lowest $^2\Sigma_g^+$ state at large values of R is in the $(1\sigma_g)(1\sigma_u)^2$ molecular configuration and becomes degenerate, in the neighborhood of $R \cong 2$ a.u., with the $(1\sigma_g)^2(2\sigma_g)$ molecular configuration which is derived from the $He^+(1s)$ and He $(1s)(2s)$ atomic states. This degeneracy is removed in the true adiabatic representation through configuration interaction. The He_2^+ lowest $^2\Sigma_g^+$ state then follows the lower curve and takes the $(1\sigma_g)^2(2\sigma_g)$ molecular configuration at values of R smaller than 2 a.u. Finally,

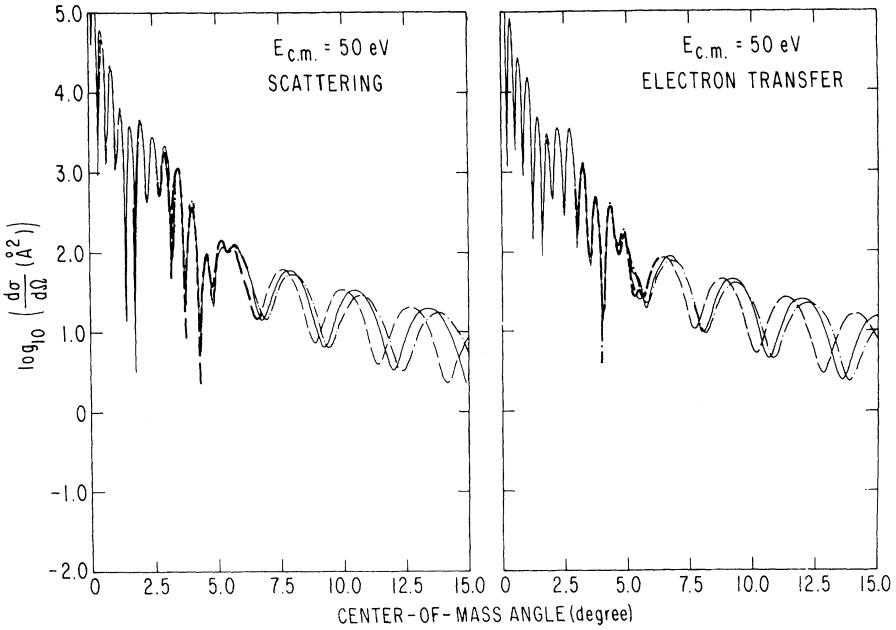

FIG. 8. Comparison of the scattering and electron-transfer differential cross sections in the absence of nuclear symmetry as functions of c.m. angle in the WKB approximation (solid line), the stationary-phase approximation with straight-line (dashed line) and angle (dot-dash line) approximations for the classical trajectory, and the eikonel approximation with straight-line (bold-face dashed line) and angle (bold-face dot-dash line) approximations for the classical trajectory for a model (He^+, He) system [Eqs. (3.1) and (3.2)] at c.m. energy of 50 eV. The differential cross sections are given in the laboratory system.

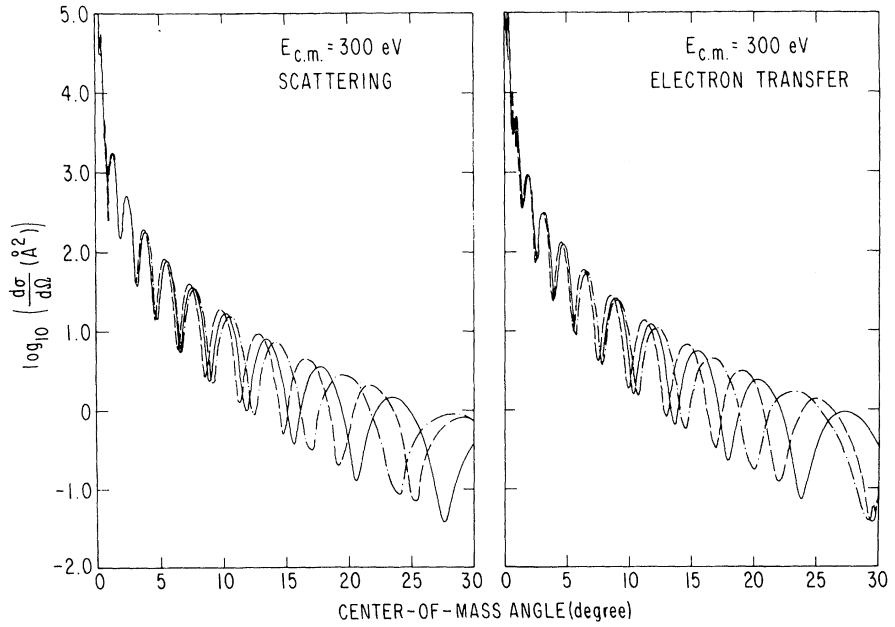

FIG. 9. Comparison of the scattering and electron-transfer differential cross sections in the absence of nuclear symmetry as functions of c.m. angle in the WKB approximation (solid line), the stationary-phase approximation with straight-line (dashed line) and angle (dot-dash line) approximations for the classical trajectory, and the eikonel approximation with straight-line (bold-face dashed line) and angle (bold-face dot-dash line) approximations for the classical trajectory for a model (He^+, He) system [Eqs. (3.1) and (3.2)] at c.m. energy of 300 eV. The differential cross sections are given in the laboratory system.

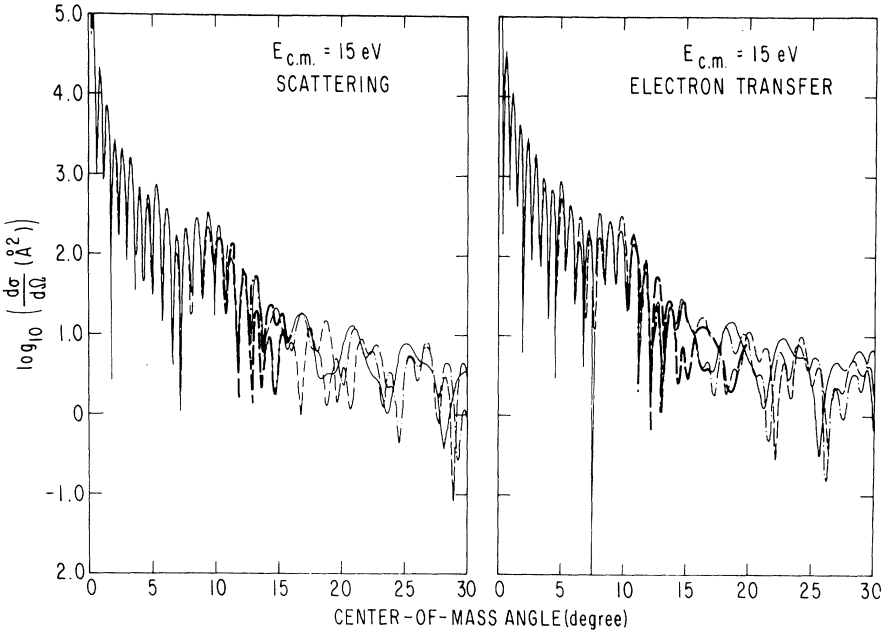

FIG. 10. Comparison of the scattering and electron-transfer differential cross sections in functions of c.m. angle in the WKB approximation (solid line), the stationary-phase approximation with straight-line (dashed line) and angle (dot-dash line) approximations for the classical trajectory, and the eikonel approximation with straight-line (bold-face dashed line) and angle (bold-face dot-dash line) approximations for the classical trajectory for a model (He^+, He) system [Eqs. (3.1) and (3.2)] at a c.m. energy of 15 eV. The differential cross sections are given in the laboratory system

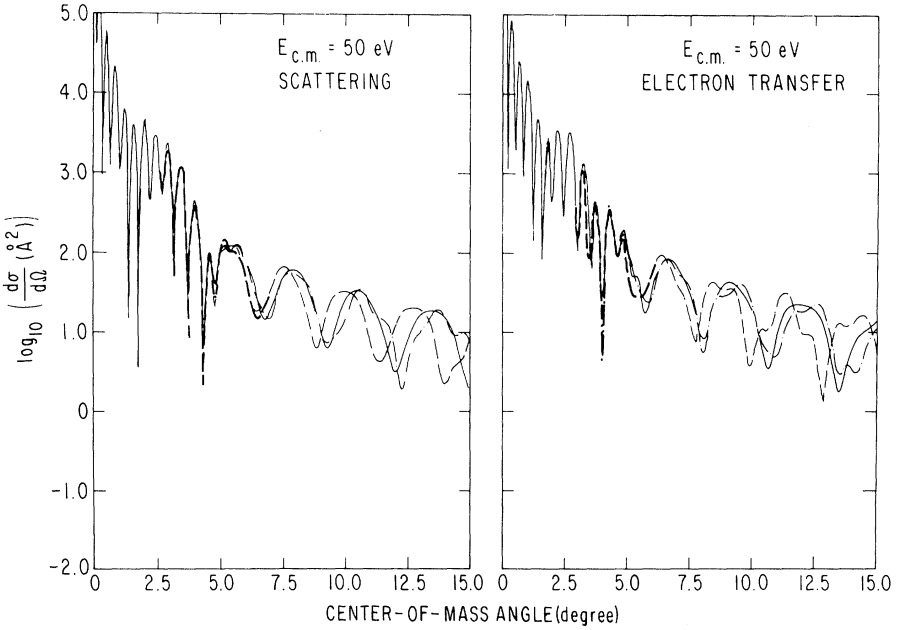

FIG. 11. Comparison of the scattering and electron-transfer differential cross sections in functions of c.m. angle in the WKB approximation (solid line), the stationary-phase approximation with straight-line (dashed line) and angle (dot-dash line) approximations for the classical trajectory, and the eikonel approximation with straight-line (bold-face dashed line) and angle (bold-face dot-dash line) approximations for the classical trajectory for a model (He^+, He) system [Eqs. (3.1) and (3.2)] at a c.m. energy of 50 eV. The differential cross sections are given in the laboratory system.

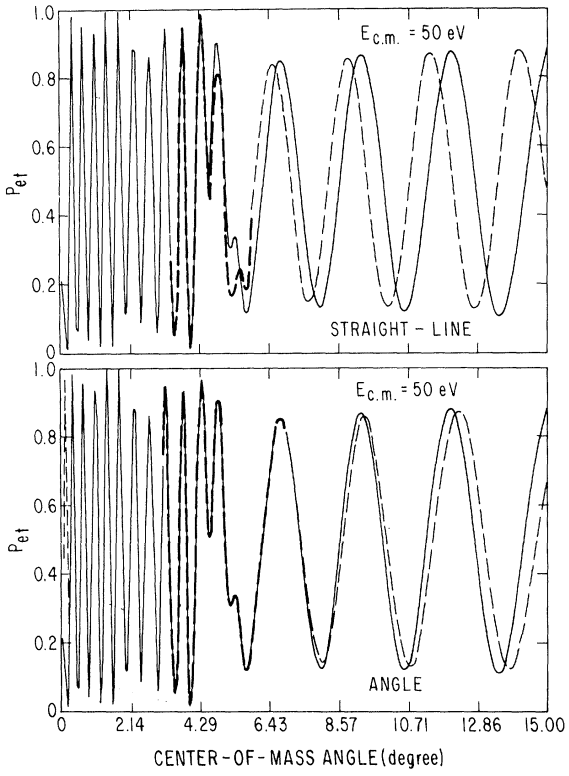

FIG. 12. Comparison of the electron-transfer probability as a function of c.m. angle in the WKB (solid line) and the stationary-phase (dashed line) and the eikonel (bold-face dashed line) approximations for a model (He^+, He) system [Eqs. (3.1) and (3.2)] at a c.m. energy of 50 eV. Calculations for the latter two approximations are reported out for both the straight-line and angle approximations for the classical trajectory.

it goes to the united-atom state $Be^+(1s)^2(2p)$.

These adiabatic potentials are found[8] to be inadequate for interpreting the detailed measurements of resonance electron-transfer probability recently reported by Lockwood, Helbig, and Everhart.[9] The most prominent feature in the measurement is that the probability does not oscillate between zero and one as predicted by the two adiabatic potentials. Bates and McCarroll[10] and Lichten[11] have indicated that the observed damping effects in the resonant electron-transfer probability resulted from the participation of excited states in the collisions.

The damping due to excited states may be accounted for either by the inclusion of these excited states in the adiabatic basis set for formulating the coupled equations to be solved or by breaking away from the adiabatic representation. The latter approach has been investigated by Lichten,[11] by F. T. Smith,[12] and by F. J. Smith.[13]

Lichten has pointed out that better agreement with experimental observation may be obtained if the He_2^+ lowest $^2\Sigma_g^+$ state is allowed to follow the upper state at values of R smaller than 2 a.u. In this case, the *gerade* He_2^+ state remains in the $(1\sigma_g)(1\sigma_u)^2$ molecular configuration at all values of R and become the $Be^+(1s)(2p)^2$ united-atom state at $R = 0$. Such a state which crosses from one state to the other is called the diabatic state.[11]

A set of diabatic interaction potentials for the interaction between ground states of He^+ and He has been constructed by Marchi and Smith,[14] and applied to the elastic He^+ on He scatterings. They have shown that the salient features observed by Lorents and Aberth[15] in the differential scattering cross section may be reasonably accounted for by the diabatic potentials. Recently a similar set of diabatic potentials have been deduced semiempirically by Olson and Mueller.[16] These sets of potentials are, however, composed of several pieces and have to be joined at joining points to preserve continuity. This can give rise to numerical difficulties.

We have constructed a set of such potentials which are in close agreement with that constructed by Marchi and Smith but have the same analytic

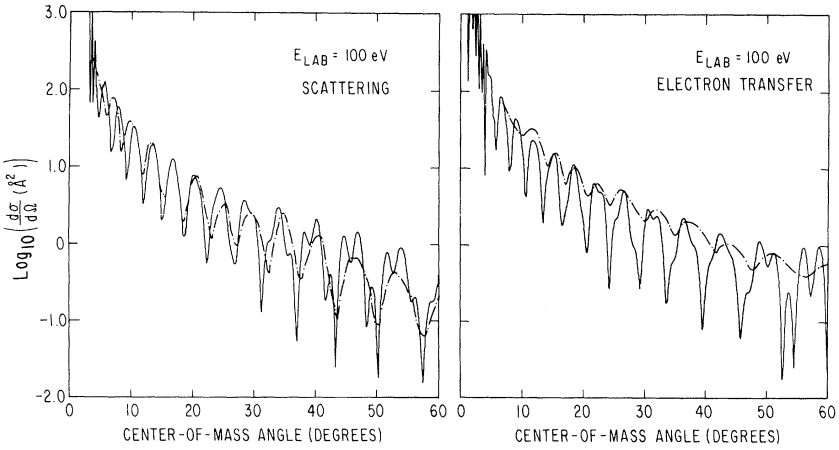

FIG. 13. Comparison of the angle dependence of the theoretical scattering and electron-transfer differential cross sections (solid line) as predicted by the model potential [Eqs. (3.1) and (3.2)] with that measured (dot-dash line) by Lorents and Aberth (Ref. 15) and by Fleischmann *et al.* (Ref. 17), respectively, at a laboratory energy of 100 eV.

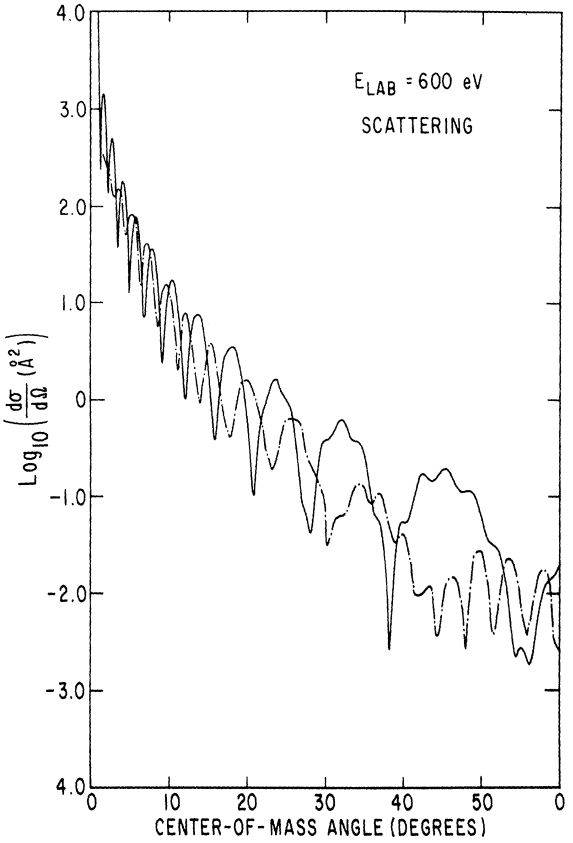

FIG. 14. Comparison of the angle dependence of the theoretical scattering differential cross sections (solid line) as predicted by the model potential [Eqs. (3.1) and (3.2)] with that measured (dot-dash line) by Lorents and Aberth (Ref. 15) at a laboratory energy of 600 eV.

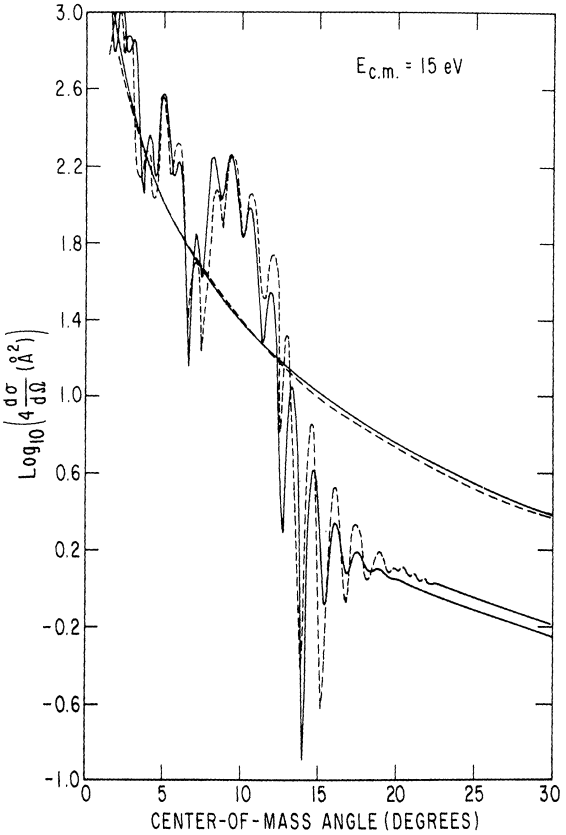

FIG. 15. Comparison of the differential cross sections for the gerade- and ungerade-potential scatterings as functions of c.m. angle predicted by the model potential (solid line) [Eqs. (3.1) and (3.2)] with that predicted by the potential deduced semiempirically by Olson and Mueller (dashed line) [Ref. 16].

forms for all internuclear distances [Eqs. (3.1) and (3.2)]. The differential scattering and electron-transfer cross sections obtained with these new potentials are compared with the experimental results of Lorents and Aberth, [15] and of Fleischmann, Young, and McGowan[17] in Fig. 13 at a c.m. energy of 50 eV. In Fig. 14 a similar comparison is made for the differential scattering cross section at a c.m. energy 300 eV. It is seen that the agreement is very good at 50 eV but becomes rather poor at 300 eV in the large scattering angle region. This kind of agreement is consistent with that obtained with the set of potentials constructed by Marchi and Smith. [14] Such a sensitive energy dependence reflects, perhaps, the dynamical nature of the diabatic states because a transition is required in order for the He_2^+ lowest $^2\Sigma_g^+$ state to cross over to the upper state in the neighborhood of $R \cong 2$ a.u. The recent work of Smith[18] on the diabatic representation may provide a better understanding of such diabatic states.

A comparison of the model potentials given by Eqs. (3.1) and (3.2) with that of Olson and Mueller is provided in Fig. 15 in which the differential cross sections for the gerade- and ungerade-potential scatterings are compared.

---

*Research supported in part by the Advanced Research Projects Agency of the Department of Defense and was monitored by the U.S. Army Research Office, Durham, under Contract No. DA-31-124-ARO-D-257, and in part by the U.S. Atomic Energy Commission and the Air Force Office of Scientific Research.

†Present address: Gordon McKay Laboratory, Harvard University, Cambridge, Mass.

[1]J. C. Y. Chen and K. M. Watson, Phys. Rev. 174, 152 (1968). This reference will be referred to as I and

equations from I referenced as Eq. (I 1.1), etc.

[2]J. C. Y. Chen and K. M. Watson, Phys. Rev. 188, 236 (1969). This reference will be referred to as II and equations from II referenced as Eq. (II 1.1), etc.

[3]G. Moliere, Z. Naturforsch. 2A, 133 (1947).

[4]K. W. Ford and J. A. Wheeler, Ann. Phys. (N.Y.) 7, 259 (1959).

[5]R. B. Bernstein, *Advances in Chemical Physics*, edited by J. Ross (Wiley-Interscience, Publishers, Inc., New York, 1966), Vol. 10, Chap. 3.

[6]G. B. Airy, Proc. Cambridge Phil. Soc. 6, 379 (1887).

[7]See for example, P. N. Reggan, J. C. Browne, and F. A. Matsen, Phys. Rev. 132, 304 (1963); B. K. Gupta and F. A. Matsen, J. Chem. Phys. 47, 4860 (1967).

[8]E. Everhart, Phys. Rev. 132, 2083 (1963).

[9]G. Lockwood, H. Helbig, and E. Everhart, Phys. Rev. 132, 2078 (1963).

[10]D. R. Bates and R. McCarroll, Advan. Phys. 11, 36 (1962).

[11]W. Lichten, Phys. Rev. 131, 229 (1963).

[12]F. T. Smith, Bull. Am. Phys. Soc. 9, 411 (1963).

[13]F. J. Smith, Phys. Letters 10, 290 (1964); Proc. Phys. Soc. (London) 84, 889 (1964).

[14]R. P. Marchi and F. T. Smith, Phys. Rev. 139, A1025 (1965).

[15]D. C. Lorents and W. Aberth, Phys. Rev. 139, A1017 (1965).

[16]R. E. Olson and C. R. Mueller, J. Chem. Phys. 46, 3810 (1967).

[17]H. H. Fleischmann, R. A. Young, and J. W. McGowan, Phys. Rev. 153, 19 (1967).

[18]F. T. Smith, Phys. Rev. 179, 111 (1969).

PHYSICAL REVIEW A VOLUME 1, NUMBER 4 APRIL 1970

Fredholm Method. I. A Numerical Procedure for Elastic Scattering

William P. Reinhardt and Attila Szabo*

Department of Chemistry, Harvard University, Cambridge, Massachusetts 02138

(Received 26 November 1969)

The Fredholm expansion of the determinant whose phase gives the elastic-scattering phase shift is "summed" by use of numerical quadrature, reducing the calculation of the phase shift to evaluation of a single finite-dimensional determinant. The method is essentially exact and is applicable, without modification, to nonlocal potentials. Results for the low-energy static and static-exchange scattering of electrons from hydrogen atoms are presented as a simple illustration of the method.

I. INTRODUCTION

The theory developed by Fredholm[1] for the solution of certain types of linear integral equations was first applied to problems in quantum scattering theory by Jost and Pais[2] in a discussion of the convergence of the Born series. They show that the Fredholm method allows the expansion of the partial-wave scattering amplitude as the ratio of two series, each of which converges absolutely for all values of the coupling parameter λ. The fact that these series converge absolutely makes them of great formal importance; however, Jost and Pais mention the fact that the method does not seem to lend itself to numerical computation, as the series may converge very slowly, except in special cases.

A remark by Schwinger[3] and subsequent development by Baker[4] rekindled interest in the Fredholm method: It may be shown that the phase of the partial-wave Fredholm determinant is directly related to the potential-scattering phase shift; as this result depends only on density-of-states arguments[5] and the use of free-particle wave functions, it is independent of ordinary Schrödinger dynamics. This latter fact suggested that the method might be useful in high-energy physics where the dynamics are largely unknown, but phenomenological potentials might be found. Newton[6] and Blankenbecler[7] have extended these potential-scattering results by giving prescriptions whereby the whole multichannel S matrix may be constructed from the Fredholm determinant. Sugar and Blankenbecler[8] have applied the method to many-particle scattering and suggested methods of attacking the three-body problem.

Numerical applications of the Fredholm method have been limited; attempts to obtain numerical results by effectively keeping only a few terms in the expansion of the Fredholm determinant have been, at best, semiquantitative.[9] For some potentials, keeping only one or two powers of λ in the expansion seems to give good results at high